Available online at www.sciencedirect.com
SCIENCE DIRECT
Catalysis Today 104 (2005) 138–148
CATALYSIS TODAY
www.elsevier.com/locate/cattod

Solid electrolyte membrane reactor for controlled partial oxidation of hydrocarbons: Model and experimental validation

Barbara Munder [a], Yinmei Ye [a], Liisa Rihko-Struckmann [a], Kai Sundmacher [a,b,*]

[a] *Max Planck Institute for Dynamics of Complex Technical Systems, Sandtorstr. 1, D-39106 Magdeburg, Germany*
[b] *Process Systems Engineering, Otto von Guericke University Magdeburg, Universitätsplatz 2, D-39106 Magdeburg, Germany*

Available online 10 May 2005

Abstract

A mathematical model of a solid electrolyte membrane reactor is presented which accounts for the prevailing physical phenomena of the electrochemical partial oxidation of *n*-butane to maleic anhydride. From an analysis of characteristic dimensionless numbers it was concluded that the reactor behaviour can be described by a one-dimensional pseudo-homogeneous approach with respect to the anodic gas channel and a one-plus-one-dimensional electrochemical model. Beside mass and charge transport processes, electrochemical charge transfer reactions as well as heterogeneously catalysed oxidation reactions are considered. As kinetic model a modified Mars–van Krevelen approach is suggested. Experimental results of oxygen pumping and butane oxidation experiments were used to determine kinetic parameters and to validate the model.

Keywords: Solid electrolyte membrane reactor; Modelling; Partial oxidation; Maleic anhydride

1. Introduction

Selective partial oxidation reactions are of major importance in industrial petrochemical production. The conversion of light hydrocarbons like alkanes to valuable products has been intensively studied in recent years. An essential and still existing problem of these reactions, however, is the low selectivity to the desired intermediate product at higher conversion. The synthesis reactions are often accompanied by the undesired but thermodynamically favoured consecutive and parallel reactions to the deep oxidation products (CO_x).

One way to improve the yield is to use porous or dense membrane reactors rather than conducting the reaction in a conventional fixed bed reactor. In a number of publications [1–3], it was shown that for favourable kinetics, if the partial pressure of oxygen appears to a lower order in the desired reaction rate than in the rate expressions for the undesired reactions, a selectivity advantage can be achieved by a controlled distributed feed of oxygen across an inert membrane. In this way, the local oxygen partial pressure can be lowered and thus the total oxidation reactions can be suppressed.

Beside the concentration, the type and state of oxygen species available at the active catalyst sites affects the reaction selectivity. Eng and Stoukides [4] and Wang and Lin [5] reported that by using dense membrane reactors the oxygen anions, O^{2-}, which are transported across the membrane, might directly form active and selective oxygen species on the membrane or the catalyst surface while gas phase oxygen, which would rather give rise to unselective reactions, could be excluded from the reaction zone.

Many studies are reported on the application of solid oxide membranes and on the electrocatalytic pathway for selective partial oxidations of hydrocarbons [6]. Whereas most of these studies focused on mixed ionic and electronic-conducting membranes (MIEC) (e.g. [7–9]), fewer investigations are reported on membrane reactors based on pure oxygen ion conducting membranes (e.g. [10–13]).

The solid electrolyte membrane reactor (SEMR) as described in [4] and [6] combines the membrane reactor concept with the working principle of a solid oxide fuel cell

* Corresponding author. Tel.: +49 391 6110351; fax: +49 391 6110353.
E-mail address: sundmacher@mpi-magdeburg.mpg.de (K. Sundmacher).

0920-5861/$ – see front matter
doi:10.1016/j.cattod.2005.03.055

A_s	geometrical surface area of anode (m^2)
A_x	cross sectional area of anode gas channel (m^2) (reactor shell side)
c_t	total molar concentration (mol m^{-3})
C_{DL}	anodic and cathodic double layer capacity (As V^{-1} m^{-2})
C^*_{DL}	dimensionless double layer capacity
C^{SE}	SE conductivity constant (A V^{-1} m^{-1})
$C^{SE,*}$	dimensionless SE conductivity constant
d^{SE}	SE membrane thickness (m)
d^{AC}	thickness of anodic catalyst layer (m)
D^{eff}	effective binary diffusion coefficient of porous anodic (m^2 s^{-1}) catalyst layer
E^j_A	activation energy for reaction j (kJ mol^{-1})
$E^{A/C}_A$	activation energy for anodic/cathodic charge transfer (kJ mol^{-1}) reaction
E^{SE}_A	activation energy for O^{2-} conduction within the (kJ mol^{-1}) SE-membrane
F	Faradays constant (96,485 As mol^{-1})
F^A	total molar flow rate within the anode gas channel (mol s^{-1})
$F^{A,0}$	total inlet molar flow rate to the anode gas channel (mol s^{-1})
$F^{A,*}$	dimensionless molar flow rate within the anode gas channel ($F^A/F^{A,0}$)
i_{cell}	cell current density (A m^{-2})
i^*_{cell}	dimensionless cell current density ($i_{cell}A_5/I_{cell,ref}$)
I_{cell}	total cell current (A)
I^*_{cell}	dimensionless cell current ($I_{cell}/I_{cell,ref}$)
$I_{cell,ref}$	reference cell current (A)
j_i	molar flow density of species i across the (mol m^{-2} s^{-1}) SE-membrane
j^*_i	dimensionless molar flow density of species i across the SE-membrane ($j_iA_5(I_{cell,ref}/F)$)
k^0_j	pre-exponential reaction rate constant for reaction j (mol kg^{-1} s^{-1})
$k^{0,*}_j$	dimensionless reaction rate constant for reaction j (mol kg^{-1} s^{-1}) (k^0_j/k^0_1)
$k^{A/C}_0$	pre-exponential reaction rate constant for (mol m^{-2} s^{-1}) anodic/cathodic charge transfer reaction
$k^{A/C,*}_0$	dimensionless reaction rate constant for anodic/(mol m^{-2} s^{-1}) cathodic charge transfer reaction ($k^{A/C}_0A_s/(I_{cell,ref}/F)$)
L	reactor length (m)
m_{Cat}	anodic catalyst weight (kg)
$q_{2/3}$	moles of oxygen required to oxidise 1 mol of n-butane/MA to CO_x
$r^{A/C}_{el}$	electrochemical charge transfer reaction rate (mol m^{-2} s^{-1}) at anode/cathode
$r^{A/C,*}_{el}$	dimensionless charge transfer reaction rate at anode/cathode ($r^{A/C}_{el}/r_{el,ref}$)
$r_{el,ref}$	reference charge transfer reaction rate (mol m^{-2} s^{-1}) ($I_{cell,ref}/A_SF$)
r_j	reaction rate of reaction j (mol kg^{-1} s^{-1})
r^*_j	dimensionless reaction rate (r_j/r_{ref})
r_{ref}	reference reaction rate, defined in Eq. (22) (mol kg^{-1} s^{-1})
R	general gas constant (8.314 J mol^{-1} K^{-1})
$R^{A/C}$	ohmic resistance of anodic/cathodic current collector (Ω)
$R^{A/C,*}$	dimensionless ohmic resistance of anodic/cathodic current collector
t	time (s)
t^*	dimensionless time (t/τ)
T	reactor temperature (K, °C)
T^*	dimensionless reactor temperature
V	volume of anode gas channel (m^3)
x_{ox}, x_{red}	mole fraction of oxidised/reduced catalyst ($x_{ox} + x_{red} = 1$)
y_i	mole fraction of species i
y^0_i	inlet mole fraction of species i
z	reactor length coordinate (m)
z^*	dimensionless reactor length coordinate (z/L)

Greek symbols

$\alpha^{A/C}$	anodic/cathodic charge transfer coefficient
β_j	kinetic order of the oxygen species in reaction j
γ_j	dimensionless activation energy, Arrhenius number, for reaction j ($E^j_A/(RT_{ref})$)
$\gamma^{A/C}$	dimensionless activation energy, Arrhenius number, for anode/cathode reaction ($E^{A/C}_A/(RT_{ref})$)
$\gamma^{S/E}$	dimensionless activation energy, Arrhenius number, for SE conductivity ($E^{SE}_A/(RT_{ref})$)
$\Delta\Phi^{A/C}$	anodic/cathodic potential difference (V)
$\Delta\Phi^{CA}$	local cell voltage ($\Phi^C - \Phi^A$) (V)
$\Delta\Phi^{SE}$	potential difference across the SE-membrane (V)
$\Delta\Phi^{k,*}$	dimensionless potential difference κ (κ: A/C/SE/CA) ($F/(RT_{ref})\cdot\Delta\Phi^k$)
$\eta^{A/C}$	anodic/cathodic overvoltage (V)
$\eta^{A/C,*}$	dimensionless anodic/cathodic overvoltage ($F/(RT_{ref})\cdot\eta^{A/C}$)
ν_{ij}	stoichiometric coefficients of species i in reaction j
σ^{SE}	conductivity of SE membrane for $O^{2(}$-ions (A $V^{(1}$ $m^{(1}$)
$\sigma^{SE,*}$	dimensionless conductivity of SE membrane for $O^{2(}$-ions

Abbreviations

A/C	anode/cathode gas channel
AC	anodic catalyst layer
Bu	n-butane
MA	maleic anhydride

HC	hydrocarbon
SE	solid electrolyte
VPO	vanadylpyrophosphate catalyst for MA synthesis

Characteristic dimensionless numbers

Da	Damköhler number ($m_{cat}r_{ref}/F^{A,0}$)
Da_{II}	second kind Damköhler number
Flr	flow ratio ($F^{A,0}/(I_{cell,ref}/F)$)
Φ	Thiele modulus

(SOFC) (Fig. 1). Oxygen and hydrocarbons are fed to the reactor at the opposing sides of a gas dense but oxygen ion conducting solid electrolyte membrane. Oxygen is reduced to O^{2-} anions at the cathode side and transported via the SE-membrane to the anode. At the anodic catalyst, hydrocarbons react with the supplied oxygen species to oxidised products. The released electrons are transported back to the cathode via the outer electric circuit.

Compared to the MIEC-membrane reactor, SEMR's allow for a direct control of the oxygen permeation rate due to the faradaic coupling of oxygen flux and cell current. Driving force of the process is the high Gibbs energy of hydrocarbon oxidation reactions, which corresponds to a positive cell voltage and allows the process to be operated in the self-driven ''fuel-cell'' mode. By applying an external potential, the oxygen feed can be further increased.

Most intensively investigated reactions in dense membrane reactors are the oxidative coupling of methane, and the partial oxidation of methane and ethane to synthesis gas and ethylene, respectively. In this study the partial oxidation of *n*-butane to maleic anhydride is chosen as model reaction, which is on the one hand as yet the only industrial application of selective oxidation of alkanes [14] and exhibits on the other hand the typical properties of partial oxidations. A recent work from our laboratory [15] shows

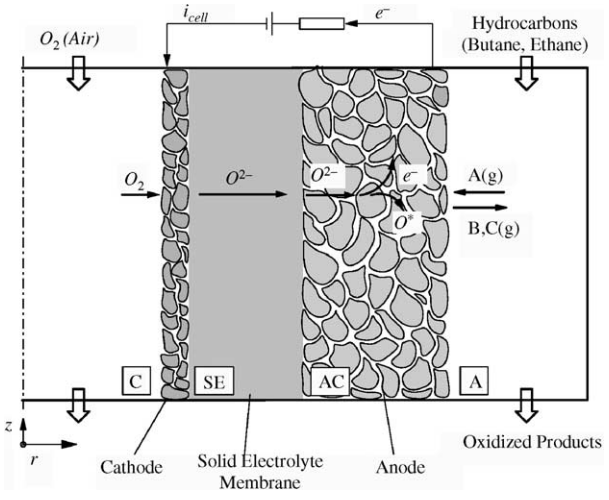

Fig. 1. Schematic diagram of the SEMR.

the feasibility of the electrocatalytic synthesis experimentally. In order to investigate the properties and to evaluate the reactor performance as well as to provide an efficient design and optimal operation conditions, a theoretical analysis and simulations are needed. However, such theoretical studies require a reliable kinetic model.

The aim of this work is to develop a mathematical model, which is capable to describe the prevailing physical phenomena taking place during the electrocatalytic maleic anhydride synthesis. Experimental data obtained with a lab scale SEMR are analysed in order to identify kinetic parameters and are further used for model validation.

2. Optimal anode design

The anodic catalyst layer of the SEMR serves both as electrode and as reaction zone for the desired selective oxidation reaction. Its design has a critical effect on the reactor performance. Thus, some detailed considerations are needed.

According to the idea of Eng and Stoukides [4] described above, ideal conditions for achieving high yields of the desired product would be provided by a single anodic electrode material, which possesses both high oxygen ion and electron conductivity and good catalytic properties for the synthesis reaction. Similar to the mixed conducting cathode in solid oxide fuel cells, the oxygen ions could diffuse on a bulk path to the active sites on the electrode surface as schematically shown in Fig. 2a. In this way, the SEMR would allow for an electrochemical modification of the catalyst surface such that the selectivity of the desired reaction is optimised.

Some recent studies report on efforts to develop such mixed conducting materials, e.g. for the oxidative coupling of methane, and on investigations of the effects of combined surface reaction and oxygen permeation (e.g. [16,17]). However, for more complicated synthesis reactions as the formation of maleic anhydride (MA), such an ideal material is hard to find. Both, the ionic and the electronic conductivity of the applied catalyst (vanadylpyrophosphate, VPO) are almost negligible as was tested in our laboratory. Therefore, a more complicated design for the anodic reaction zone is required. The MA synthesis catalyst has to be either mixed with an electron conductor (typically a metal) and an oxygen ion conductor (e.g. YSZ) to form a composite electrode, which is coated on top of the catalytically inactive solid electrolyte membrane (commonly YSZ) (Fig. 2b). Or alternatively, a separate electron-conducting layer can be placed between the solid electrolyte and a layer of the synthesis catalyst as depicted in Fig. 2c. In all three cases, the complete anodic catalyst layer has to be porous in order to allow for a sufficient contact area between the gas phase and the solid materials.

The last configuration is of the three the easiest to be practically established and was, therefore, chosen for our first experimental investigations.

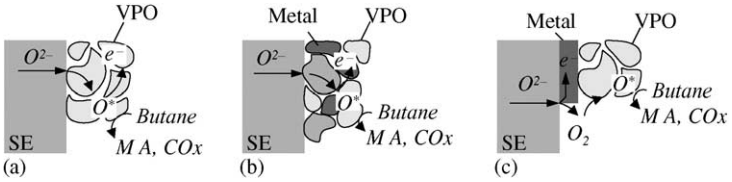

Fig. 2. Anode design options: (a) mixed conducting electrode; (b) composite electrode; and (c) bilayer electrode, and resulting oxygen transport paths to the active sites.

3. Model formulation

3.1. Kinetic model

Despite the fact that selective oxidation on dense solid oxide membranes is widely investigated only a few kinetic studies and kinetic model considerations can be found. Wang and Lin [5] used for their theoretical work on the oxidative coupling of methane on dense mixed conducting membranes a parallel-series reaction mechanism where methane is activated and oxidised by lattice oxygen while gas phase oxygen promotes the total oxidation. In solid oxide fuel cells (when operated in the direct oxidation mode without steam reforming), the hydrocarbon fuel is considered to be directly electrochemically oxidised to CO_2 converting the Gibbs energy of reaction (minus some losses due to the inner cell resistances) into electric energy.

The partial oxidation of *n*-butane to maleic anhydride, however, is rather a complicated synthesis reaction, with the overall reaction given in Eq. (1).

$$C_4H_{10} + 3.5O_2 \xrightarrow{VPO} C_4H_{10}O_3 + 4H_2O \quad (1)$$

The only known catalyst that promotes the reaction is vanadylpyrophosphate $(VO)_2P_2O_7$ (VPO), which to our knowledge does not exhibit electrocatalytic properties. Thus, as a first approach we assume that the maleic anhydride synthesis in a SEMR takes place on the same route as in conventional catalytic reactors. Preceding molecular oxygen is released to the gas phase by the electrochemical charge transfer reaction as is schematically depicted in Fig. 2c.

The reaction kinetics of the conventional (non-electrochemical) *n*-butane oxidation to maleic anhydride over a VPO catalyst has been intensively studied over a wide range of operation conditions during the past years [18–22]. An extensive overview on proposed kinetic models was recently given by Lorences et al. [19]. Most of them apply a simplified triangular (or a slightly adapted triangular) reaction network, as shown in Fig. 3, and their kinetic equations are of the Mars–van Krevelen or Eley–Rideal type redox mechanism. However, a generally accepted model, which can be applied to a wide range of operation conditions, does not yet exist. In particular the kind of active oxygen species, O^*, on the catalyst surface, which is responsible for selective and unselective oxidation steps as well as the role of gaseous oxygen, is not known so far. Some researchers introduce two kinds of active sites on the VPO catalyst surface into their models [19,21], which promote the MA formation or the deep oxidation, respectively, while others consider just one active site [20]. However, both models seem to predict experimental results with similar accuracies [19].

Since there is still so much uncertainty on the kinetic model, we started our considerations in this study with a simple Mars–van Krevelen type kinetic. The reaction pathway is of the parallel-series type as shown in Fig. 3. In detail, the selective formation of MA, Eq. (2), as well as the butane and MA decomposition to CO_x, Eqs. (3) and (4), take place by consuming catalyst lattice oxygen. There is just one single kind of oxygen species, O^*, available on the active sites, namely Cat_{ox}.

$$C_4H_{10} + 7Cat_{ox} \rightarrow C_4H_2O_3 + 4H_2O + 7Cat_{red} \quad (2)$$

$$C_4H_{10} + q_2Cat_{ox} \rightarrow 4CO_x + 5H_2O + q_2Cat_{red} \quad (3)$$

$$C_4H_2O_3 + q_3Cat_{ox} \rightarrow 4CO_x + H_2O + q_3Cat_{red} \quad (4)$$

The reduced catalyst is afterwards re-oxidised by gaseous oxygen, Eq. (5),

$$Cat_{red} + \tfrac{1}{2}O_2 \rightarrow Cat_{ox} \quad (5)$$

which is supplied electrochemically, Eqs. (6) and (7), as described above.

$$\text{Cathode}: \quad \tfrac{1}{2}O_2 + 2e^- \rightleftarrows O^{2-} \quad (6)$$

$$\text{Anode}: \quad O^{2-} \rightleftarrows \tfrac{1}{2}O_2 + 2e^- \quad (7)$$

For simplicity, the total oxidation products CO and CO_2 are lumped together as was reported by other researchers (e.g. [19]). Side reactions on other active oxygen species might occur but are neglected for this study.

The rates of the electrochemical charge transfer reactions can be described by a Butler–Volmer Eq. (8).

$$r_{el}^{A/C} = k_0^{A/C}\exp\left(-\frac{E_A^{A/C}}{RT}\right)\left[\exp\left(\frac{\alpha^{A/C}nF}{RT}\eta^{A/C}\right) - (y_{O_2})^{0.5}\exp\left(-\frac{(1-\alpha^{A/C})nF}{RT}\eta^{A/C}\right)\right] \quad (8)$$

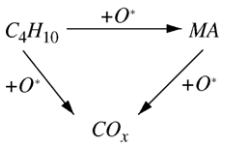

Fig. 3. Simplified triangular reaction network for butane oxidation (O^*: Cat_{ox}, O_{ad}, $O_{2,ad}$, O^-, O^{2-}, O_2(g), etc.).

For the reactions (2)–(5), rate expressions are derived according to the Mars–van Krevelen mechanism, Eq. (9), assuming a quasi-steady-state for the intermediate lattice oxygen species, Cat_{ox}, as well as a first kinetic order with respect to its concentration, x_{ox}

$$r_j = k_j^0 \exp\left(\frac{E_A^j}{RT}\right) y_{HC} x_{ox} = k_j y_{HC} \frac{1}{1 + \sum_j K_j (y_{HC}/y_{O_2})} \quad (9)$$

3.2. Reactor model

The following physical phenomena have to be considered in a SEMR. Through the solid electrolyte membrane (SE, in Fig. 1) charge in form of the oxygen anions, O^{2-}, is transported by migration. Due to geometrical reasons, the membrane thickness is some orders of magnitude smaller than the surface dimensions, the current flows predominantly in radial direction.

On the inner surface of the anodic catalyst layer (AC), both the electrochemical charge transfer reactions and the heterogeneously catalysed gas phase reactions take place. The reactions are coupled with diffusive mass transport through the pores and with charge transport in form of oxygen anions, O^{2-}, and electrons, e^-, through the solid phase of the catalyst layer, respectively. Both, the gas phase diffusion and the oxygen ion transport are predominantly in radial direction, whereas the electrons are moved in axial direction. Finally, in the anodic gas channel (A) mass transport can be convective and diffusive.

Assuming plug flow along the anodic gas channel (A) without axial dispersion and neglecting possible radial concentration profiles in a first approach, the complete system can be modelled by a model one-dimensional with respect to the gas channel and one-plus-one-dimensional with respect to the solid electrolyte membrane and the porous catalyst layer (AC).

Prior to any calculation, dimensionless numbers can be used to pre-estimate the influence of the internal mass transfer resistances within the anodic catalyst layer. The second kind Damköhler number, Da_{II}, which is also known as the square of the Thiele modulus, gives an estimate of the ratio of the reaction rates to the diffusion rate under characteristic conditions and is defined as

$$Da_{II} = \Phi^2 = \frac{(d^{AC})^2 r_{ref} m_{Cat}}{D^{eff} c_t V} \quad (10)$$

where r_{ref} stands for a (intrinsic) reference reaction rate as defined below in Eq. (22). In the range of operating conditions typically applied for MA synthesis (T = 350–550 °C), kinetic parameters as given in the literature [22] ($k_1(T) = 0.1 - 10\,\mathrm{mol\,kg_{Cat}^{-1}\,s^{-1}}$), and a catalyst layer thickness in the range of 0.1–1 mm, values for Da_{II} of less than 10^{-2} can be expected. This means, the gas diffusion resistance inside the catalyst pores can be rather neglected due to the slow catalytic reactions and the process takes place in the reaction kinetic controlled regime.

We defined a second Da_{II}^{el} number for the ratio of a characteristic electrochemical reaction rate to a characteristic O^{2-} migration rate through the solid phase of the AC layer as

$$Da_{II}^{el} = \frac{d^{AC} r_{el,ref} F}{\sigma_{O^{2-}}^{eff} \Delta\Phi_{max}} \quad (11)$$

Even if a composite material as described above is used as anode and the ion-conductivity is estimated to be as high as 0.01 S m^{-1}, values for Da_{II}^{el} bigger than 10 will be reached due to the low operation temperature. As a result, the electrochemical charge transfer reactions take place confined to a very narrow region close to the membrane surface.

From the above considerations, one can conclude that under the given operation conditions the process is practically divided into two locally separated parts. The first comprises all charge transport processes and the electrochemical charge transfer reactions within the SE membrane and a narrow surface region of the electrodes. The second covers all gas phase transport processes and catalytic gas phase reactions. Due to the low diffusion resistances, the anode gas channel and the anodic catalyst layer can be combined and modelled by a one-dimensional pseudo-homogeneous approach. The processes in this combined region are coupled with the electrochemical processes via the radial oxygen flow.

Further assumptions are made as follows. The reactor is operated under isothermal conditions, which can be assumed to be valid due to the low reactant concentrations applied and the temperature control provided by the experimental set-up. The pressure drop along the gas channels is neglected, and the gas phases obey the ideal gas law. The cathodic side is assumed to be a quasi-steady state oxygen reservoir, which can be experimentally established by a sufficiently high air flow rate through the cathode channel (C). Interfacial mass transfer resistances between the gas phases and solid surfaces of the membrane layers are even smaller than the diffusion resistances in the catalytic layers and can, therefore, be neglected as well. Adsorption and desorption processes might have an influence but are not taken into consideration in this work.

On the basis of these assumptions, the following model equations are obtained. The component balances for the gas phase species i (i: Bu, MA, CO_x, H_2O, O_2) on the anode side yield

$$c_t \frac{\partial y_i}{\partial t} = -\frac{1}{A_z} \frac{\partial (F^A y_i)}{\partial z} + \frac{A_s}{V} j_i + \frac{m_{cat}}{V} \sum_j \nu_{ij} r_j \quad (12)$$

with the initial conditions

$$y_i(z, t=0) = y_{i,0}$$
$$y_i(z=0, t) = y_i^0$$

The assumed isobaric conditions and the ideal gas law lead to a quasi-static mass balance for the anodic gas phase

$$0 = -\frac{1}{A_z}\frac{\partial F^{\mathrm{A}}}{\partial z} + \frac{A_s}{V}\sum_i j_i + \frac{m_{\mathrm{cat}}}{V}\sum_i\sum_j \nu_{ij} r_j \tag{13}$$

with

$$F^{\mathrm{A}}(z=0,t) = F^{\mathrm{A},0}$$

The flow density $J_i(z)$ obeys Faradays law for oxygen, and is equal to zero for all other gas phase components.

$$j_i(z) = \begin{cases} \frac{1}{2} r_{\mathrm{el}}^{\mathrm{A}} & i : \mathrm{O_2} \\ 0 & i : \mathrm{Bu, MA, CO_x, H_2O} \end{cases} \tag{14}$$

The electrochemical processes can be represented by an equivalent circuit as illustrated in Fig. 4. Charge balances characterise the anodic and the cathodic potential difference across the interfaces between the electrolyte and the respective electrode.

$$\frac{\partial \Delta\Phi^{\mathrm{A}}}{\partial t} = \frac{\partial \eta^{\mathrm{A}}}{\partial t} = \frac{1}{C_{\mathrm{DL}}}(i_{\mathrm{cell}} - 2F r_{\mathrm{el}}^{\mathrm{A}}) \tag{15}$$

$$\frac{\partial \Delta\Phi^{\mathrm{C}}}{\partial t} = \frac{\partial \eta^{\mathrm{C}}}{\partial t} = \frac{1}{C_{\mathrm{DL}}}(-i_{\mathrm{cell}} - 2F r_{\mathrm{el}}^{\mathrm{C}}) \tag{16}$$

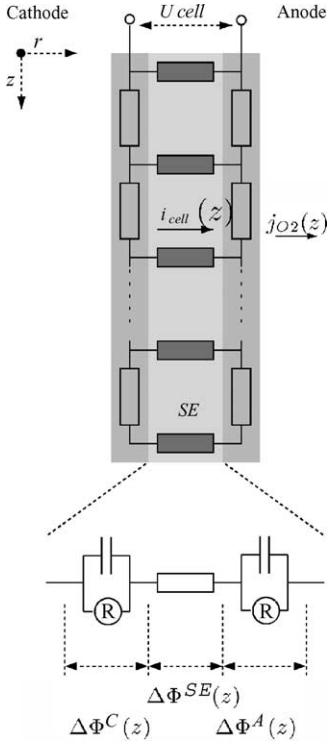

Fig. 4. Equivalent circuit representing the electrochemical model of the SEMR.

Ohm's law describes the potential drop across the solid electrolyte as well as along the electrodes.

$$\Delta\Phi^{\mathrm{SE}} = \frac{d^{\mathrm{SE}}}{\sigma^{\mathrm{SE}}(T)} i_{\mathrm{cell}} \tag{17}$$

$$\frac{\partial \Delta\Phi^{\mathrm{CA}}}{\partial z} = (R^{\mathrm{A}} + R^{\mathrm{C}})\frac{A_s}{L^2}\int_{\tilde{z}=z}^{\tilde{z}=L} i_{\mathrm{cell}}\,\mathrm{d}\tilde{z} \tag{18}$$

The local potential difference between cathode and anode at each point along the z-coordinate is calculated according to Kirchhoff's law (Fig. 4.)

$$\begin{aligned}\Delta\Phi^{\mathrm{CA}} &= \Delta\Phi^{\mathrm{C}} - \Delta\Phi^{\mathrm{SE}} - \Delta\Phi^{\mathrm{A}} \\ &= \Delta\Phi_{00}^{\mathrm{CA}} + \eta^{\mathrm{C}} - \Delta\Phi^{\mathrm{SE}} - \eta^{\mathrm{A}}\end{aligned} \tag{19}$$

The cathodic and anodic overpotentials, η^{A} and η^{C}, are defined such that both activation and concentration effects are included.

Last, the integral of current densities over the reactor length must be equal to the total cell current,

$$I_{\mathrm{cell}} = \frac{A_s}{L}\int_{z=0}^{z=L} i_{\mathrm{cell}}\,\mathrm{d}z \tag{20}$$

and a modified Arrhenius type equation is applied for the temperature dependence of the SE-membrane conductivity

$$\sigma^{\mathrm{SE}}(T)T = C^{\mathrm{SE}}\exp\left(-\frac{E_{\mathrm{A}}^{\mathrm{SE}}}{RT}\right) \tag{21}$$

The model variables are made dimensionless with respect to the total inlet flow rate $F^{\mathrm{A},0}$, the reactor length L, a reference temperature, and a reference reaction rate, which is defined as

$$r_{\mathrm{ref}} = r_1(T, y_{\mathrm{Bu}} = 1.0, x_{\mathrm{ox}} = 1.0) = k_1(T) \tag{22}$$

Additionally, a reference cell current is chosen such that under characteristic feed conditions oxygen and butane are fed at the stoichiometric feed ratio of 3.5 with respect to MA formation. The complete set of dimensionless model equations can be found in Table 1.

The partial differential equations are discretised, and the resulting DAE system of first-order ODEs and algebraic equations is implemented and solved by a LIMEX solver within the simulation environment DIVA, a dynamic simulator for chemical engineering plants (University of Stuttgart, Germany).

Although within this work only stationary simulations are performed, the model equations are implemented in their dynamic form, both to account for the preferred model structured for the dynamic simulator and to allow for later dynamic simulations.

4. Parameter identification and model validation

In order to validate the model and to get values for the unknown reaction rate constants and SE conductivity parameters, several series of experiments were conducted.

Table 1
Dimensionless model equations

Anodic gas channel and catalyst layer (i: butane, MA, CO_x, H_2O, O_2):	
Component mass balances	$\frac{\partial y_i}{\partial t^*} = -\frac{\partial (F^{A,*} y_i)}{\partial z^*} + \frac{1}{Flr} j_i^* + Da \sum_j \nu_{ij} r_j^*$
Total mass balance	$0 = -\frac{\partial F^{A,*}}{\partial z^*} + \frac{1}{Flr} \sum_i j_i^* + Da \sum_i \sum_j \nu_{ij} r_j^*$
Initial conditions	$y_i(z, t=0) = y_{i,0}$
	$y_i(z=0, t) = y_i^0$
	$F^{A,*}(z=0, t) = 1.0$
Flow density	$j_i^*(z) = \begin{cases} \frac{1}{2} r_{el}^{A,*} & i: O_2 \\ 0 & i: Bu, MA, CO_x, H_2O \end{cases}$
Electrochemical model:	
Charge balances	$\frac{\partial \Delta\Phi^{A,*}}{\partial t^*} = \frac{1}{C_{DL}^*}(i_{cell}^* - 2r_{el}^{A,*})$
	$\frac{\partial \Delta\Phi^{C,*}}{\partial t^*} = \frac{1}{C_{DL}^*}(-i_{cell}^* - 2r_{el}^{C,*})$
Ohm's law	$\Delta\Phi^{SE,*} = \frac{i_{cell}^*}{\sigma^{SE,*}(T)}$
	$\frac{\partial \Delta\Phi^{CA,*}}{\partial z^*} = (R^{A,*} + R^{C,*}) \int_{\tilde{z}=z^*}^{\tilde{z}=1} i_{cell}^* d\tilde{z}$
Local cell voltage	$\Delta\Phi^{CA,*} = \Delta\Phi^{C,*} - \Delta\Phi^{SE,*} - \Delta\Phi^{A,*}$
Total cell current	$I_{cell}^* = \int_{z^*=0}^{z^*=1} i_{cell}^* dz^*$
Arrhenius-type equation	$\sigma^{SE,*}(T^*)T^* = C^{SE,*} \exp\left(-\frac{\gamma^{SE}}{T^*}\right)$
Reaction kinetics:	
Charge transfer reactions	$r_{el}^{A/C,*} = k_0^{A/C,*} \exp\left(-\frac{\gamma^{A/C}}{T^*}\right)\left[\exp\left(\frac{\alpha n}{T^*}\eta^{A/C,*}\right) - y_{O_2}^{0.5} \exp\left(-\frac{(1-\alpha)n}{T^*}\eta^{A/C,*}\right)\right]$
Non-electrochemical reactions	$r_j^* = k_j^{0,*} \exp\left(\frac{1}{T^*}(\gamma_1 - \gamma_j)\right) y_{HC} x_{ox}^{\beta j}$

The details of the experimental set-up are given in [15] and [25]. In brief, we used a tubular lab scale reactor, which was coated on the tube side with platinum as cathodic catalyst and on the anodic (shell) side by a gold/VPO catalyst bilayer. As solid electrolyte yttria-stabilised-zirconia (13 mol% YSZ) was used with a thickness of about 400 μm. The reactor was operated in an electric oven under temperature control, thus isothermal conditions could be established. The *n*-butane/inert gas mixture was fed to the shell side while air was circulated through the tube side. The reactor outlet concentrations were monitored by an online-gas-chromatograph, and the cell current was adjusted with a galvanostat. The butane feed concentrations were in the range of 0.5–1.2 vol.%, and the temperature between 450 and 550 °C.

4.1. Solid electrolyte conductivity

The first set of experiments was dedicated to determine the temperature dependence of the oxygen anion O^{2-} conductivity through the solid electrolyte membrane (13%YSZ). The measurements were carried out by the two-probe AC impedance spectroscopy using a symmetric cell configuration (Air, Pt||YSZ (13%)||Pt, Air) ([15]). The experimental set-up ensured a homogeneous current density. The experimental data published in [15] were used to determine the conductivity constant, C^{SE}, and the activation enthalpy, E_A^{SE}, by a least square fit of the modified Arrhenius-type Eq. (21). The fitting results for both parameters are listed in Table 2. Fig. 5 shows the experimental data as well as the simulated conductivity as function of the inverse temperature.

From these results, one finds values for the oxygen conductivity of the SE membrane between 0.04 and 0.24 S m^{-1} within the temperature range of 450–550 °C as applied for butane oxidation. Assuming an allowable potential drop across the SE membrane of maximal 2.0 V, the highest molar oxygen fluxes that can be reached are 0.5 and 3.0 mmol m^{-2} s^{-1}, respectively.

4.2. Kinetic parameters of electrochemical reactions

The characteristic isothermal current–voltage behaviour obtained from oxygen pumping experiments can be analysed in order to determine the unknown kinetic parameters for the electrochemical reactions (Eqs. (6) and (7)). Ye et al. [25] will publish the data as well as the experimental conditions

Table 2
SE conductivity parameters and kinetic parameters of electrochemical reactions

$C^{SE} = 2.8 \times 10^8$ S K m^{-1}
$E_A^{SE} = 96.9 \times 10^3$ J mol^{-1}
$k_0^A = 1.46 \times 10^3$ mol m^{-2} s^{-1}
$k_0^C = 1.46 \times 10^4$ mol m^{-2} s^{-1}
$E_A^{A/C} = 200 \times 10^3$ J mol^{-1}
$\alpha^{A/C} = 0.3$

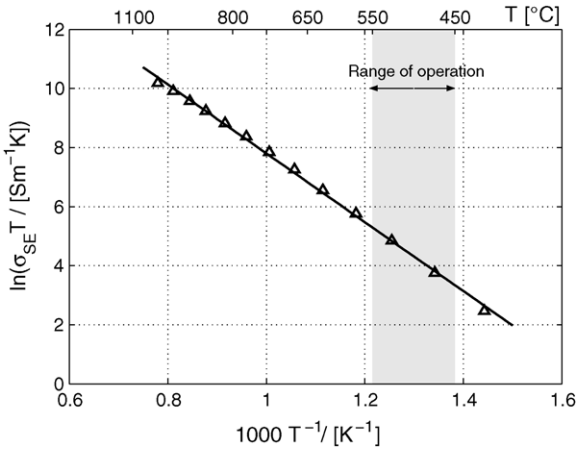

Fig. 5. Modified Arrhenius plot of measured and simulated solid electrolyte conductivity.

in detail. In brief, the measurements were conducted at two temperatures (473 and 520 °C) at the upper and lower limits of the operational range for butane oxidation. The reactor configuration was the tubular SEMR described above with a Pt–Ag composite cathode and a gold layer on the anodic side as electrocatalysts. While on the cathodic side the air flow was maintained, the anodic gas channel was supplied with pure nitrogen. The experimental set-up did not include a reference electrode thus the cathodic and the anodic charge transfer processes could not be measured separately. Since the Pt–Ag composite material is known to have much better electrocatalytic properties for the electrochemical oxygen reduction, Eqs. (6) and (7), we estimated a value of 10 for the ratio of the cathodic to the anodic exchange current density and assumed the activation energies as well as the charge transfer coefficients to be equal.

Under these assumptions, the parameters of the Butler–Volmer kinetics, Eq. (8), $k_0^{A/C}$, $E_A^{A/C}$, $\alpha^{A/C}$ were determined by a least-square optimisation using the SEMR model developed above. The fitted curves for both series of measurements are shown in Fig. 6a and the obtained parameters are given in Table 2. The results are taken as an estimate for the kinetic parameters. Additional measurements at further temperatures as well as experiments in a SEMR with a properly placed reference electrode are in preparation and will be conducted in the near future.

At this point, some qualitative conclusions can be drawn. High voltages had to be applied to the reactor to attain a mean current density along the reactor length as low as 10–20 A m^{-2}. For comparison, in solid oxide fuel cells, values of 2000–4000 A m^{-2} are reached at similar cell voltages. The main reason for the low current densities is the low temperature, which has to be applied for the maleic anhydride synthesis in the SEMR but leads to an exponential rise of both the SE-membrane conduction resistance and the resistances of the charge transfer reactions. Fig. 6b shows a simulation of the partial cell overvoltages at the operation temperature of 473 °C. It was found that not the oxygen ion

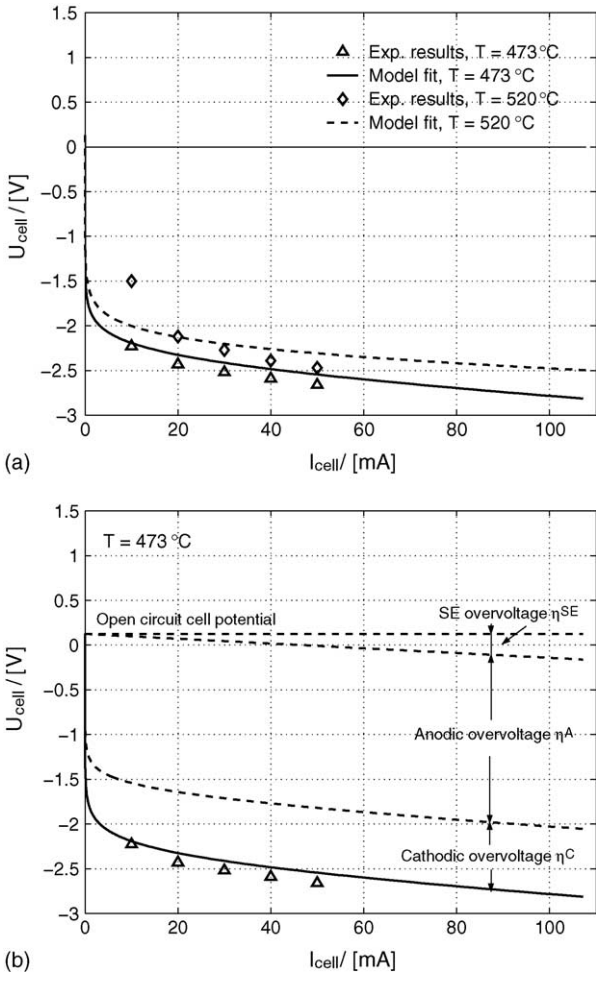

Fig. 6. Characteristic isothermal current–voltage behaviour of the SEMR obtained from oxygen pumping experiments: (a) as function of temperature; and (b) analysis of partial cell overvoltages (geometrical surface area $A_s = 23$ cm^2).

conduction through the SE-membrane but the anodic and the cathodic charge transfer reactions contribute the major part to the high voltage drop. This means, however, that a significantly lower cell resistance cannot be achieved by employing thinner SE-membranes. Instead, the electrocatalytic performance and/or the design of the electrodes have to be improved. The possibly most critical part is the electric contact between the electrodes and the electrolyte, which have to be tightly fixed.

4.3. Kinetic parameters of gas phase reactions

The SEMR model described above was used to simulate the reactor behaviour under butane oxidation conditions and the results were compared with experimental data obtained in our laboratory [25]. From first simulations, we found significant deviations between model predictions and experiments when using kinetic parameters directly from the literature [22] for the gas phase reactions (2)–(5). There are two obvious reasons. First, the kinetic parameters were

determined by Hess [22] partly under different operation conditions and had, therefore, to be extrapolated for our application. Second, in contrast to a co-feed fixed bed reactor as applied in [22], during SEMR operation, there might different active oxygen species on the electrolyte or metal surface exist, which significantly influence the reaction rates but were not observed by Hess. In particular, the experimentally observed dependence of the (integral) MA selectivity on the cell current, or the oxygen-to-butane feed ratio, respectively (see Ye et al. [25]), showing a slight maximum could not be reproduced by the model.

In order to better describe our experimental results, we, therefore, modified the kinetic model equations. Retaining the assumed reaction mechanism, the Mars–van Krevelen type rate expressions given in Eq. (9) for the reactions (2)–(5) were altered by introducing reaction orders, β_j, different to 1.0 with respect to the concentration of the active oxygen species, x_{ox}, as shown in Eq. (23). The assumption of a first reaction order with respect to the hydrocarbon species was kept as was suggested, e.g. by Lorences et al. [19] for low butane and MA concentrations.

$$r_j = k_j y_{HC} x_{ox}^{\beta_j} \tag{23}$$

Furthermore, the quasi-steady-state assumption for the intermediate lattice oxygen species was adopted from the original Mars–van Krevelen approach, thus the following implicit algebraic equation was obtained and added to our model equations.

$$\underbrace{k_4 y_{O2}^{0.5}(1-x_{ox})^{\beta 4}}_{\text{Catalyst reoxidation}} = \underbrace{7k_1 y_{Bu} x_{ox}^{\beta 1}}_{\text{MA formation}} + \underbrace{q_2 k_2 y_{Bu} x_{ox}^{\beta 2}}_{\text{Butane total oxidation}} + \underbrace{q_3 k_3 y_{MA} x_{ox}^{\beta 3}}_{\text{MA total oxidation}} \tag{24}$$

With this modified kinetic approach, the differential selectivity for MA is given by

$$S_{MA,diff}(z) = \frac{r_1 - r_3}{r_1 + r_2} = \frac{1 - (k_3/k_1)(y_{MA}(z)/y_{Bu}(z)) x_{ox}^{(\beta 3 - \beta 1)}(z)}{1 + (k_2/k_1) x_{ox}^{(\beta 2 - \beta 1)}(z)} \tag{25}$$

If one takes into account that the reducing character of the reaction mixture decreases along the axial reactor coordinate and hence, the mole fraction of oxidised catalyst, x_{ox}, monotonically increases along z, the modified kinetic approach would allow to predict a maximum of the integral MA selectivity as function of the oxygen-to-butane feed ratio with an appropriate set of parameters ($\beta_3 < \beta_1 < \beta_2$ or $\beta_2 < \beta_1 < \beta_3$, respectively).

The results of steady-state butane oxidation experiments in the SEMR (Ye et al. [25]) were used to estimate the kinetic parameters for Eq. (24). The available measurements were conducted under isothermal galvanostatic operation at various cell currents, temperatures, butane inlet concentrations, and residence times (flow rates) in the anodic gas channel, as those are the most important operational parameters that influence the reactor performance.

The carbon balance was found to be well fulfilled (>95%) as was checked by considering the measured reactor outlet concentrations of the carbon containing gas phase species, i.e. butane, MA, and CO_x. The production of further side products like butene and furan was negligible, and also carbon deposition on the catalyst surface was not observed in significant amounts.

In order to reduce the number of adjustable parameters, the activation enthalpies, $E_{A,j}$, for all reactions were initially adopted from Hess [22]. By fitting the experimental reactor outlet concentrations of butane and maleic anhydride simultaneously for all experiments, the values for the remaining constants, k_j^0, and β_j, were determined. The obtained parameters are summarised in Table 3. Fig. 7 shows the fitted curves for butane conversion, MA selectivity, and MA yield together with experimental results as function of the oxygen-to-butane feed ratio. Additionally, the selectivity curve for CO_x, which was calculated assuming the carbon balance to be completely fulfilled, is added to Fig. 7b and compared with measured results.

Generally, we found a good agreement between experimental results and simulations. The increasing butane conversion and, resulting, the increasing MA yield for rising oxygen-to-butane feed ratios up to 1.4 are well reproduced. The prediction of the (integral) MA selectivity is improved in comparison to the original kinetic model. However, there is a notable difference between measurement and simulation for oxygen-to-butane feed ratios below 0.5. Even with the modified kinetic approach, the model simulations could not reproduce the observed maximum of the integral MA selectivity.

The determined values for the reaction orders, β_j, with respect to the concentration of the active oxygen species, x_{ox}, show the expected trend for partial oxidation reactions, i.e. the reaction order for the desired MA formation, β_1, appears to a lower value than the reaction order β_2 for the total oxidation of butane. The value β_3 for the combustion of MA, however, was found to be the lowest of the three. Thus, at very low oxygen or catalyst lattice oxygen concentrations, x_{ox}, respectively, the

Table 3
Kinetic parameters of gas phase reactions

	Hess [22]	This work
k_1^0(kmol g_{cat}^{-1} s^{-1})	0.056	0.512
k_2^0(kmol g_{cat}^{-1} s^{-1})	0.713	8.605
k_3^0(kmol g_{cat}^{-1} s^{-1})	22.4	227.5
k_4^0(kmol g_{cat}^{-1} s^{-1})	1.88	10.0
$E_{A,1}$(kj mol^{-1})	80.0	80.0
$E_{A,2}$(kj mol^{-1})	92.0	92.0
$E_{A,3}$(kj mol^{-1})	113.0	113.0
$E_{A,4}$(kj mol^{-1})	102.0	102.0
β_1	1.0	0.71
β_2	1.0	1.03
β_3	1.0	0.48
β_4	1.0	1.0

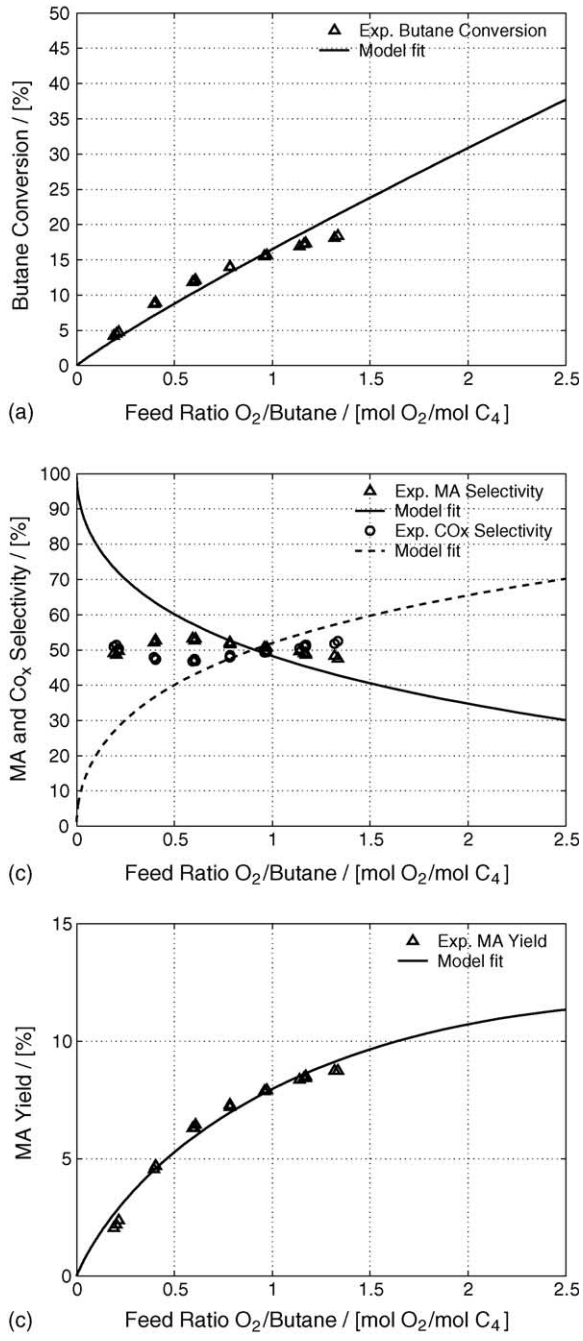

Fig. 7. Experimental and simulated results as function of the oxygen-to-butane feed ratio ($T = 480$ °C, $F^{A,0} = 32$ ml min^{-1}(NTP), $y^0_{Bu} = 0.0056$, $m_{Cat} = 165$ mg).

consecutive reaction of MA to CO_x was accelerated compared to the desired reaction leading to a lower MA selectivity. However, due to the low butane conversion within the considered oxygen feed range, the MA concentration reached only values of less than 10% of the local butane concentration. The rate constant $k_3(T)$ for the MA combustion, on the other hand, was only about 2 to 3 times higher than $k_1(T)$ for the desired reaction within the investigated temperature range (450–550 °C). Hence, the consecutive reaction of MA to CO_x was of minor importance. By testing the parameter sensitivities we found the simulation results only little affected by variations of the reaction order β_3, which supports the last conclusion. The differential selectivity for MA is thus determined by the simplified equation

$$S_{MA,diff}(z) = \frac{1}{1 + (k_2/k_1)x_{ox}^{(\beta 2-\beta 1)}(z)} \quad (26)$$

which leads to the monotonically decreasing intergral selectivity as function of the oxygen-to-butane feed ratio shown in Fig. 7b.

The slight decline of the integral MA selectivity for low oxygen-to-butane feed ratios could, therefore, still not be reproduced. A further modification of the kinetic model seems to be necessary. Possibly, the assumption of constant reaction kinetics and reaction orders over the entire range of operation conditions was not applicable. Under the strongly reducing atmospheres at oxygen-to-butane feed ratios below 0.5, the reaction orders could have changed or the catalyst could have been deactivated, which was not taken into consideration by the model.

In order to check the assumed values for the activation enthalpies, E_{Aj}, we simulated the dependence of butane

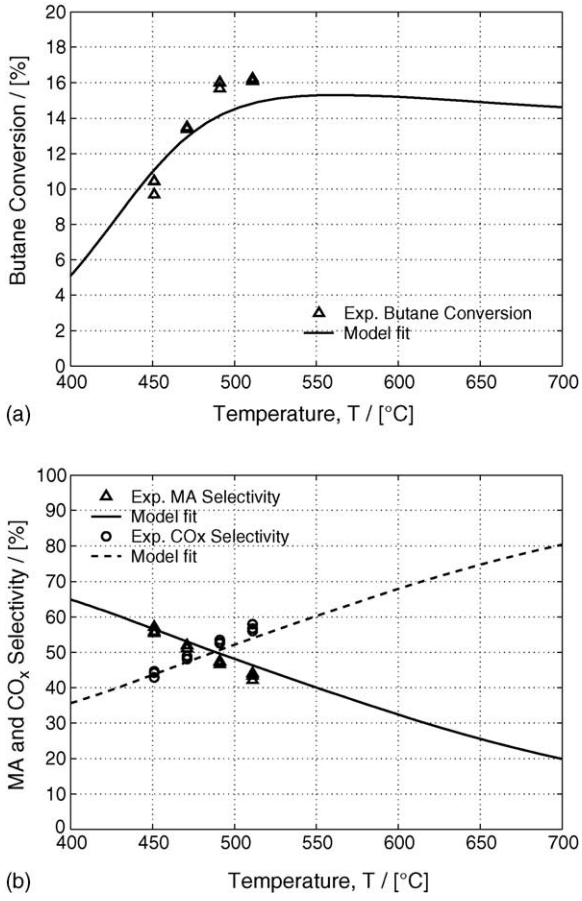

Fig. 8. Experimental and simulated results as function of temperature (oxygen-to-butane feed ratio = 0.8, $F^{A,0} = 32$ ml min^{-1}(NTP), $y^0_{Bu} = 0.0056$).

conversion and MA selectivity on the reactor temperature based on the determined parameter set in Table 3 and compared the curves with experimental results as shown in Fig. 8. Here, we found a good agreement within the experimentally investigated range. The activation enthalpies reported in [22] could be thus confirmed. The slight decline of the butane conversion for temperatures above 550 °C occured due to the depletion of oxygen, which was the stoichiometric limiting component in all measurements [25], and a simultaneous increase in the CO_x selectivity with rising temperatures. Because a higher oxygen-to-butane ratio was needed for CO_x formation compared to the ratio of 3.5 for the MA formation, less butane could thus be converted.

The reaction rate constants obtained in this work were about 10 times higher than the respective literature values from [22]. A possible reason could be a different activity of the VPO catalyst used in our work compared to that applied by Hess. Additionally, further oxygen species on the metal electrode (Au) or the solid electrolyte membrane surface during the SEMR operation might have contributed to the higher conversion rates as discussed above. The selectivity for maleic anhydride obtained in the SEMR was, however, comparable or slightly lower than reported, e.g. by Mallada [23] for the conventional (non-electrochemical) conversion of *n*-butane to MA. Liu et al. [24] report in their review paper about similar observations for the oxidative coupling of methane in a SEMR. Here, the electrochemically pumped oxygen was found to be more active than gas phase oxygen, but less selective for the desired reaction and mainly the total oxidation was enhanced.

5. Conclusions

A mathematical model of a solid electrolyte membrane reactor applied for the partial oxidation of *n*-butane to maleic anhydride was formulated. From anode design and kinetic considerations we concluded that the complex synthesis of MA takes place rather on the same route as in conventional catalytic reactors than on an electrocatalytic pathway while oxygen is supplied electrochemically across the SE-membrane. By analysing the two characteristic dimensionless numbers, Da_{II} and Da_{II}^{el}, it was shown that for the slow catalytic MA synthesis the reactor behaviour can be modelled by a one-dimensional pseudo-homogeneous approach with respect to the anodic gas channel and a one-plus-one-dimensional model with respect to the electrochemical processes. The electrochemical charge transfer reactions were found to take place within a very narrow region of the porous anode.

Experimental results from oxygen pumping and butane oxidation experiments were used to estimate the unknown kinetic parameters of electrochemical reactions and gas phase reactions and to validate the developed model. A modified Mars–van Krevelen kinetic model was derived. With that, a generally good agreement between simulated and experimental data was found for oxygen-to-butane ratios above 0.5. For lower feed ratios the model overestimated the MA selectivity.

Although the main research focus should be rather on higher oxygen-to-butane feed ratios since only those are of practical interest, an analysis of the low feed ratio range could possibly reveal an interesting insight into the reaction mechanism and the concentration dependencies. For a future work, further modifications of the kinetic approach are in preparation, which account for selective and nonselective sites on the catalyst surface as suggested, e.g. in [19] as well as consider the direct electrochemical oxidation route.

References

[1] S.C. Reyes, E. Iglesia, C.P. Kelkar, Chem. Eng. Sci. 48 (14) (1993) 2643–2661.
[2] Y. Lu, A.G. Dixon, W.R. Moser, Y.H. Ma, Chem. Eng. Sci. 52 (8) (1997) 1349–1363.
[3] C. Hamel, S. Thomas, K. Schädlich, A. Seidel-Morgenstern, Chem. Eng. Sci. 58 (19) (2003) 4483–4492.
[4] D. Eng, M. Stoukides, Catal. Rev. Sci. Eng. 33 (3–4) (1991) 375–412.
[5] W. Wang, Y.S. Lin, J. Membr. Sci. 103 (1995) 219–233.
[6] M. Stoukides, Catal. Rev. Sci. Eng. 42 (1–2) (2000) 1–70.
[7] F.T. Akin, Y.S. Lin, J. Membr. Sci. 209 (2002) 467–475.
[8] F.T. Akin, Y.S. Lin, AIChE J. 48 (10) (2002) 2298–2306.
[9] Y. Lu, A.G. Dixon, W.R. Moser, Y.H. Ma, U. Balachandran, J. Membr. Sci. 170 (2000) 27–34.
[10] S. Hamakawa, K. Sato, T. Hayakawa, A.P.E. York, T. Tsunoda, K. Suzuki, M. Shimizu, K. Takehira, J. Electrochem. Soc. 144 (1) (1997) 1–5.
[11] K. Takehira, T. Shishido, S. Hamakawa, H. Kajioka, Solid State Ionics 152–153 (2002) 641–646.
[12] G. Xui-Mei, K. Hidajat, C.B. Ching, Ind. Eng. Chem. Res. 36 (1997) 3576–3582.
[13] G. Xui-Mei, K. Hidajat, C.B. Ching, Catal. Today 50 (1999) 109–116.
[14] G. Centi, F. Cavani, F. Trifiro, Selective Oxidation by Heterogeneous Catalysis, Kluwer Academic/Plenum Publishers, New York, 2001.
[15] Y. Ye, L. Rihko-Struckmann, B. Munder, H. Rau, K. Sundmacher, Ind. Eng. Chem. Res. 43 (2004) 4551–4558.
[16] A. Löfberg, S. Boujmiai, E. Capoen, M.C. Steil, C. Pirovano, R.N. Vannier, G. Mairesse, E. Bordes-Richard, Catal. Today 91–92 (2004) 79–83.
[17] F.T. Akin, J.Y.S. Lin, J. Membr. Sci. 231 (2004) 133–146.
[18] R. Mallada, Estudio de la Oxidación Selective de Butano a Anhídrido Maleico en Reactores de Membrana, Ph.D. thesis, University of Zaragoza, Zaragoza, Spain, 1999.
[19] M.J. Lorences, G.S. Patience, F.V. Diez, J. Coca, Ind. Eng. Chem. Res. 42 (2003) 6730–6742.
[20] J.S. Buchanan, S. Sundaresan, Appl. Catal. 19 (1985) 65–75.
[21] S.K. Bej, M.S. Rao, Ind. Eng. Chem. Res. 30 (1991) 1829–1832.
[22] S. Hess, Kinetische Untersuchung zur getrennten Reaktionsführung der selektiven Butan-Oxidation, Ph.D. thesis, University of Erlangen, 2002.
[23] R. Mallada, M. Menéndez, J. Santamaría, Catal. Today 56 (2000) 191–197.
[24] S. Liu, X. Tan, K. Li, R. Hughes, Catal. Rev. 43 (1–2) (2001) 147–198.
[25] Y. Ye, L. Rihko-Struckmann, B. Munder, K. Sundmacher, Appl. Catal. A. 285 (2005) 86–95.